High-Frequency Microwave Detection With GaN HEMTs in the Subthreshold Regime

Gaudencio Paz-Martínez, Ignacio Íñiguez-De-La-Torre, Philippe Artillan, Héctor Sánchez-Martín, Sergio García-Sánchez, Tomás González, Javier Mateos

High-Frequency Microwave Detection with GaN HEMTs in the Subthreshold Regime

Gaudencio Paz-Martínez, Ignacio Íñiguez-de-la-Torre, Philippe Artillan, Héctor Sánchez-Martín, Sergio García-Sánchez, Tomás González, *Senior Member, IEEE,* and Javier Mateos, *Member, IEEE*

***Abstract*—The behaviour of GaN-based high electron mobility transistors (HEMTs) as microwave zero-bias detectors is very dependent on the configuration of the bias (current or voltage), the operation temperature and whether the radio-frequency power is fed in the drain or the gate terminal. When the signal is injected into the drain, the negative current responsivity shows a bell-shape dependence on V_{GS} centered slightly above the threshold voltage for all the studied frequencies (1 to 43 GHz) and temperature ranges (8 to 400 K). In the case of the voltage responsivity, depending on the temperature range (associated to the presence or absence of drain leakage current), an increase or decrease of the responsivity is observed in subthreshold conditions. For the gate-injection configuration, as expected by the capacitive gate-drain coupling, the voltage responsivity at low frequency is null, but only for V_{GS} above threshold. Surprisingly, in subthreshold conditions it is very high and positive, contrary to the negative values intuitively expected for this configuration. The origin of this unexpected behavior, taking place in both gate and drain injection configurations, is that the drain terminal is self-biased at the zero-current operating point (V_{DS} being largely negative). An analytical model based on static coefficients obtained from DC measurements is able to explain the mechanisms behind the observed dependencies of the experiments.**

***Index Terms*—Device physics, GaN high electron mobility transistors (HEMTs), Radio frequency detection, Responsivity model, Subthreshold, Zero-bias detector**

I. Introduction

In the last few years, high electron mobility transistors (HEMTs) based on AlGaN/GaN have been investigated for applications such as broadband communications [1], radar components [2] or space applications [3] because of their excellent frequency and power characteristics. In this work, AlGaN/GaN HEMTs are applied as microwave detectors in the mm-wave region over a wide range of temperatures [4], [5]. In [6] and [7], a complete review of the state-of-the-art of FET-based THz detectors and their applications is presented. We focus our attention on their properties as zero-bias detectors, where excess noise is avoided and no self-heating takes place.

Manuscript received 3 August 2023; revised 18 October 2023; accepted 9 November 2023. Date of publication 23 November 2023; date of current version 5 June 2024. This work was supported in part by MCIN/AEI/10.13039/501100011033 under Grant PID2020-115842RB-I00. *(Corresponding author: Gaudencio Paz-Martínez)*

G. Paz-Martínez, I. Íñiguez-de-la-Torre, Héctor Sánchez-Martín, Sergio García-Sánchez, T. González and J. Mateos are with with the Applied Physics Department, and USAL-NANOLAB, Universidad de Salamanca, 37008 Salamanca, Spain (e-mail: gaupaz@usal.es, indy@usal.es, hectorsanchez-martin@usal.es, sergio_gs@usal.es, tomasg@usal.es, javierm@usal.es).

P. Artillan is with Univ. Grenoble Alpes, Univ. Savoie Mont Blanc, CNRS, Grenoble INP, IMEP-LAHC, 38000 Grenoble, France (e-mail: philippe.artillan@univ-smb.fr).

GaN-based HEMT devices, because of the presence of defects, may present temperature effects, like negative threshold voltage shifts [8], degradation of the device characteristics in high temperatures [9] and dissimilar behavior in a wide range of temperature operation. In particular, as we will show, when operating as microwave detectors, the behavior of the responsivity may significantly change with temperature depending on the ionization degree of acceptors in the buffer [10]. For a complete analysis, four different configurations must be considered, depending on whether current or voltage is detected (with short- or open-circuit drain terminal, respectively) and whether the RF power is injected into the drain or gate terminal, which we will denote as Drain-Injection (DI) and Gate-Injection (GI) configurations, respectively.

Voltage detection in the subthreshold region shows a complex behavior due to drain self-biasing, which can be very significant when the transistor has a proper pinch-off behavior [5]. Indeed, in the presence of drain leakage current through the buffer (as happens in GaN HEMTs at low T due to the non ionization of the acceptor ions of the buffer), the DI voltage responsivity in sub-threshold conditions becomes almost null, instead of being high as expected for "good" transistors. However, while the subthreshold behavior within the DI configuration was well explained in [5], the GI case is not yet well understood. Some works have shown that the voltage response is suppressed in the subthreshold region due to loading or leakage current effects [11], [12], [13], but a general explanation of the detection mechanism in GI configuration is still lacking. In this contribution, using expressions for the responsivity based on the Taylor series expansion of the I_D-V_{DS} curves [14], [15], we are able to retrieve and explain the experimental results in all the different configurations where V_{DS} self-biasing plays a key role. While the Taylor series expansion can be used to represent both nonlinear current and charge sources of the devices [16], our approach is just based on static current coefficients.

II. Device Under Test and Experimental Setup

We focus our study on a AlGaN/GaN HEMT (inset in Fig. 2) grown on a high-resistivity silicon substrate whose details are provided in [5], [17], [10]. The skecth of the experimental setup is presented in Fig. 1, a LakeShore CRX-VF cryogenic probe station is used to perform the measurements in a temperature range of 8-400 K. The layout contains co-planar-waveguide (CPW) accesses to contact the terminals with GSG RF probes. A VNA Keysight N5244A has been used as RF

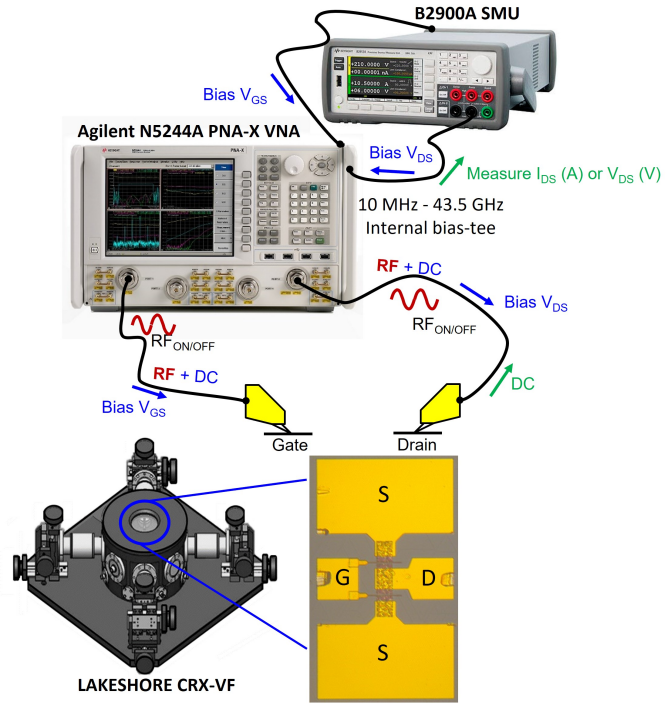

Fig. 1. Experimental setup, a cryogenic probe station is used to connect the VNA and the SMU to the device under test (the photography is presented in the sketch) trough a GSG RF probes.

power source up to 43 GHz. The insertion losses of the cables ad tips have been taken into account to actually deliver a constant RF power, P, at the reference plane of the transistor. The microwave signal in a 1 to 43 GHz span is injected either into the drain or the gate terminals. In order to bias both the gate and the drain of the transistor, a two-channel SMU B2902A is used. Two different modes for zero-bias detection will be used: zero-current (ZC) with open-circuit drain, and zero-voltage (ZV) with short-circuit drain. The responsivity in ZC conditions is obtained as the ratio $\beta_v = \frac{\Delta V}{P}$ and in ZV is $\beta_i = \frac{\Delta I}{P}$, where ΔV and ΔI are the DC shift caused by the RF excitation recorded always at the drain terminal and averaged during 5 s. Subscripts d or g are added to distinguish between DI and GI (β_{vd}, β_{vg}, β_{id} and β_{ig}).

III. Results and Discussion

Fig. 2 shows the $I_D - V_{GS}$ curves and the corresponding transconductance g_m for a transistor with L_G=250 nm and W=2×25 μm with V_{DS}=0.1 V in the 8-400 K temperature range. At low T, up to 100 K, the current and g_m, as well as the threshold voltage (V_{th}), hardly depend on temperature [5]. Above, I_D and g_m decrease with increasing T, and also V_{th}.

The ZV current responsivity in both DI and GI configurations *vs.* V_{GS} always shows a bell shape with a maximum located 0.2-0.3 V above V_{th} and goes down to zero in subthreshold conditions regardless of T, Figs. 3(a) and (b). However, while β_{id} is flat at low frequency and then shows a high frequency roll-off (results not shown here, see [17], [18]), β_{ig} is suppressed at low frequency due to the capacitive gate-drain coupling (the RF power needs to reach the drain in order

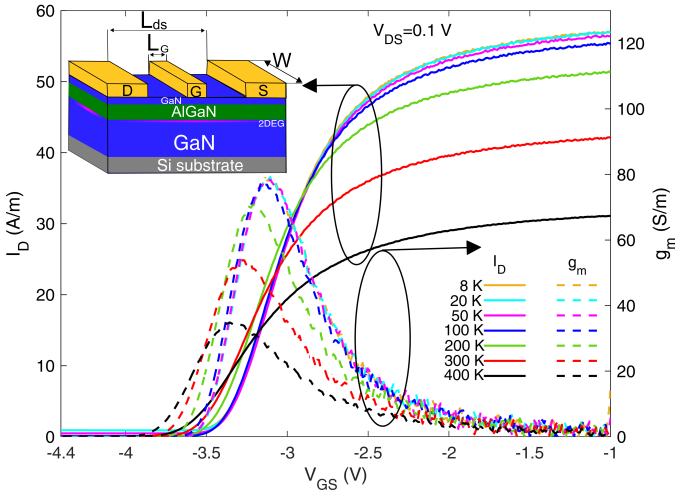

Fig. 2. $I_D - V_{GS}$ (left axis) and corresponding transconductance g_m (right axis) of the HEMT under study for V_{DS}=0.1 V and temperatures from 8 to 400 K. A scheme of the transistor geometry is shown in the inset.

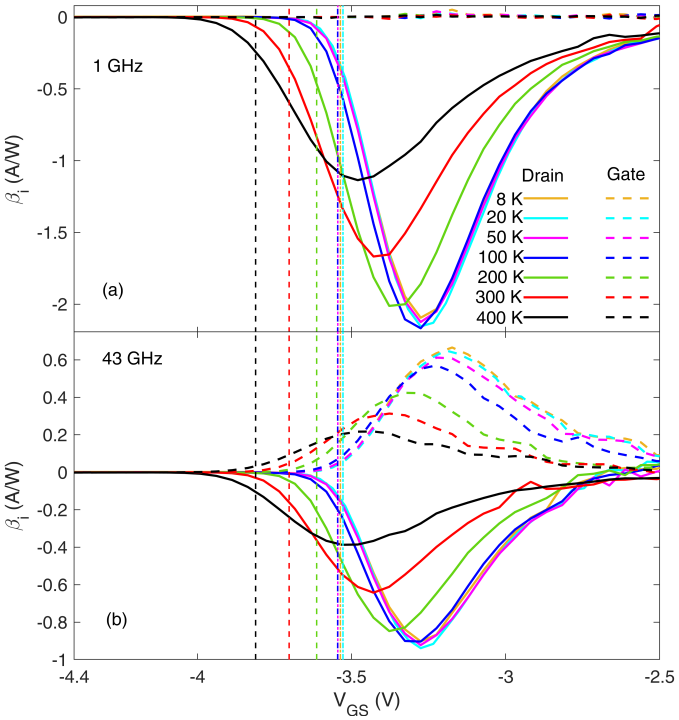

Fig. 3. Zero-voltage (ZV) current responsivity (in A/W) measured at (a) 1 GHz and (b) at 43 GHz as a function of V_{GS} using both DI and GI configurations in the 8-400 K temperature range. The dashed vertical lines indicated the values of V_{th} for each temperature. The experiments were made with a small input RF power of -15 dBm injected to a GaN-HEMT with L_G=250 nm and W=2×25 μm.

to produce a non-zero response [18]). It is also remarkable that DI and GI configurations provide responses with opposite sign, see Fig. 3(b).

In the case of the ZC voltage responsivity, Figs. 4(a) and (b), for T <200 K, β_{vd} exhibits a bell shape with a positive maximum near V_{th}, being practically null in the subthreshold region, while for T >200 K it increases and saturates for $V_{GS} < V_{th}$. The origin of this behaviour was already explained

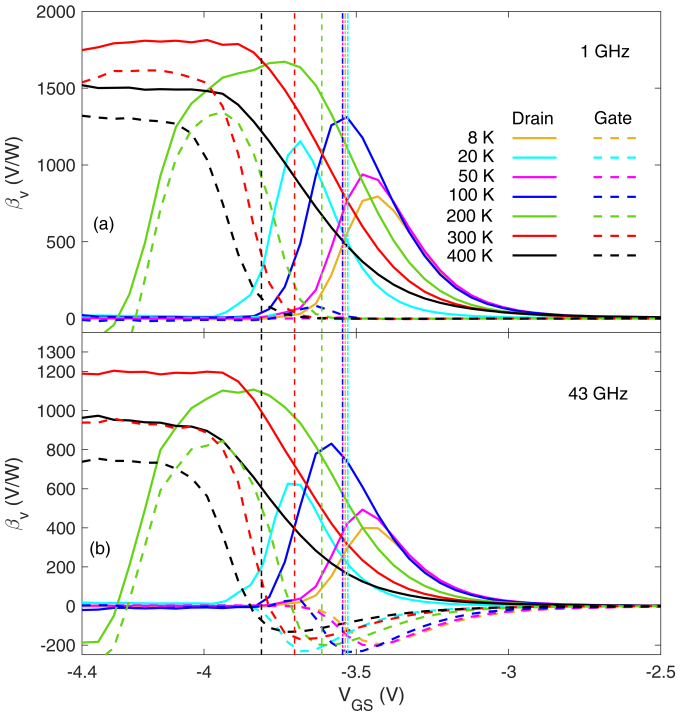

Fig. 4. Zero-current (ZC) voltage responsivity (in V/W) measured at (a) 1 GHz and (b) 43 GHz as a function of V_{GS} using both DI and GI configurations in the 8-400 K temperature range. The dashed vertical lines indicate the values of V_{th} for each temperature. The experiments were made with a small RF input power of -15 dBm injected to a GaN-HEMT with L_G=250 nm and W=2×25 μm.

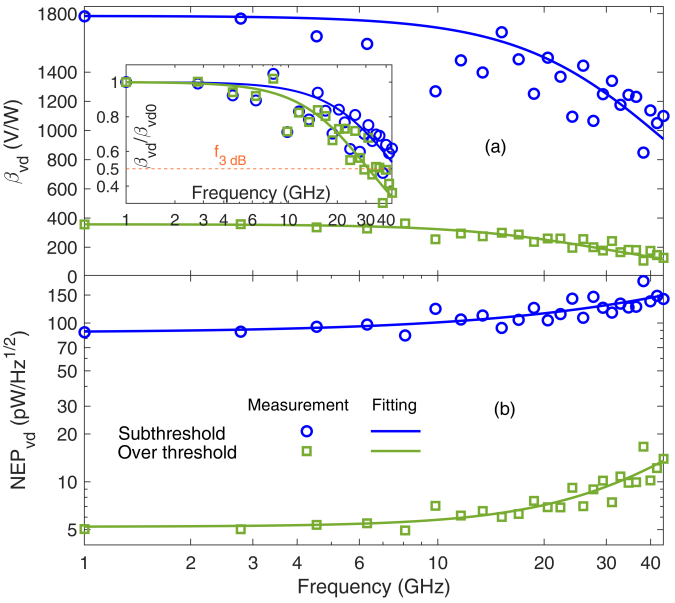

Fig. 5. (a) Zero-current (ZC) responsivity at 300 K in DI for two values of V_{GS}: in subthreshold, V_{GS} =-4.28 V $< V_{th}$, and above threshold near pinch-off , V_{GS} =-3.61 V $> V_{th}$. The inset shows the normalized β_{vd} measurements (symbols) and data fittings (lines) to Lorentzians in order to extract the cutoff frequency. (b) The NEP value for each case.

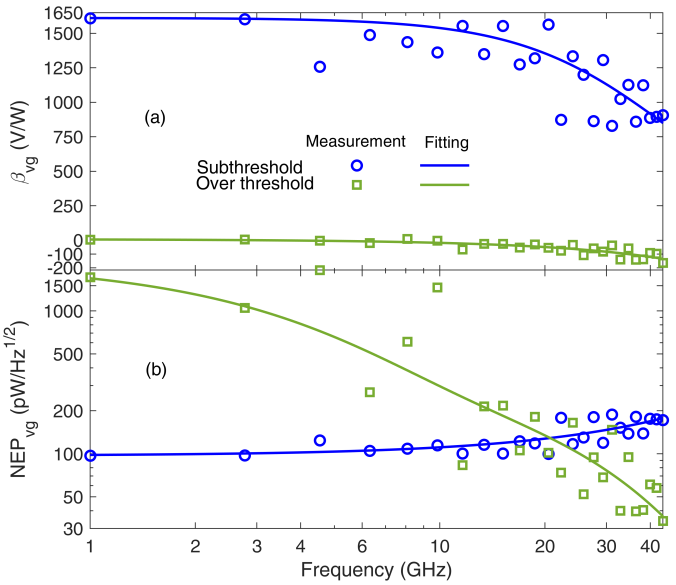

Fig. 6. (a) Zero-current (ZC) responsivity at 300 K in GI for two values of V_{GS}: in subthreshold, V_{GS} =-4.28 V $< V_{th}$, and above threshold near pinch-off , V_{GS} =-3.61 V $> V_{th}$. (b) The NEP value for each case.

in [5]. It is due to the p-type doping of the GaN buffer, which is not active at low T, thus leading to an enhancement of the drain leakage current. In fact, a good transistor pinch-off leads to the self-biasing of the drain terminal due to the I_D=0 bias condition, which is only fulfilled for negative V_{DS}, with the transistor entering into the *third-quadrant-conduction* region to generate a non-zero I_D able to compensate the always present (even if very small) gate leakage current. The most significant result of Fig. 4 is the behavior shown by β_{vg} in the subthreshold region for T >200 K. Surprisingly, β_{vg} takes large positive values at 1 GHz, while a null value is expected due to the negligible gate-drain coupling at low frequency. In addition, the sign change of β_{vg} at high frequency was unexpected (see the transition of V_{GS} through V_{th} in Fig. 4(b)). In [10] measurements of both responsivities over a wide temperature range are presented within DI configuration for devices with different gate lengths.

In order to better understand the origin of these unexpected results, the frequency dependence of the ZC voltage responsivity at 300 K is plotted in Fig. 5(a) for DI and 6(a) for GI for two different bias points, one near pinch-off (but with the HEMT still conducting), V_{GS} =-3.61 V $> V_{th}$, and the other corresponding to subthreshold conditions, V_{GS} =-4.28 V $< V_{th}$. For DI [Fig. 5(a)], in both cases β_{vd} shows a low-frequency plateau and then a high-frequency roll-off which will be characterized by its 3 dB frequency, f_{3dB}, for which a halved responsivity is obtained. The inset in Fig. 5(a) shows the $1/(1+(f/f_{3dB})^2)$ fitting. A value for f_{3dB} of 47 GHz is found in subthreshold conditions, much higher than that for $V_{GS} > V_{th}$, 31 GHz. On the other hand, in the case of GI, Fig. 6(a), clear differences between the two operation regions are observed:

- For V_{GS} above threshold β_{vg} is null at low frequencies (up to ≈10 GHz), where it starts increasing. This high-pass filter behavior is that expected for the GI configuration, since the gate-drain coupling is purely capacitive.
- In subthreshold conditions the frequency dependence of β_{vg} resembles that obtained in DI, with a similar f_{3dB}.

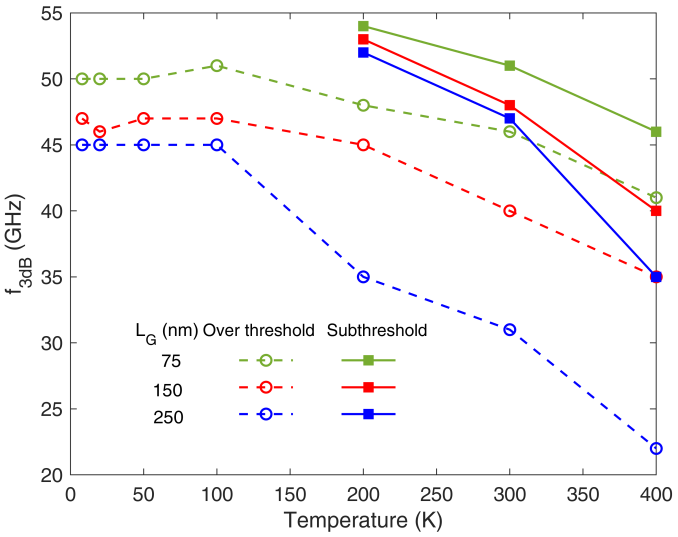

Fig. 7. Comparison of f_{3dB} for DI as a function of temperature for subthreshold (square symbol) and over threshold (circle symbol) gate bias conditions for three lengths of the gate, L_G.

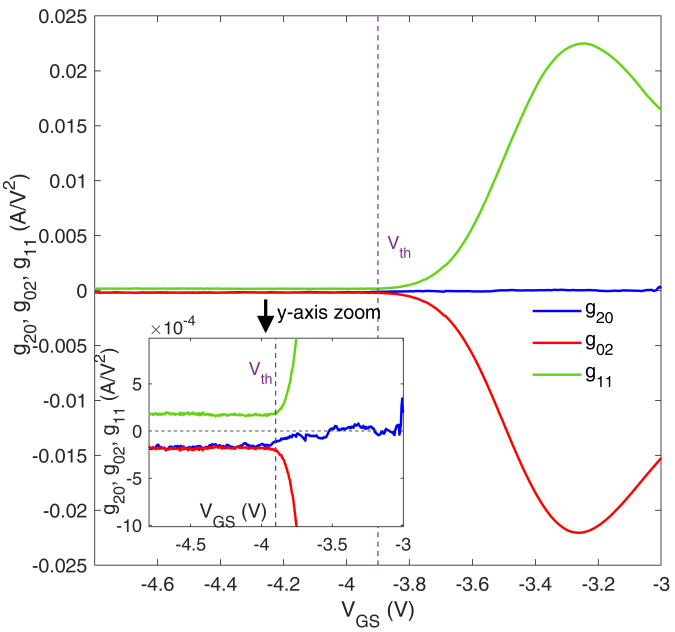

Fig. 8. Taylor series coefficients g_{02}, g_{20} and g_{11} vs. V_{GS} at 300 K. The vertical dotted line indicates the value of V_{th}. The inset corresponds to a zoom around the threshold.

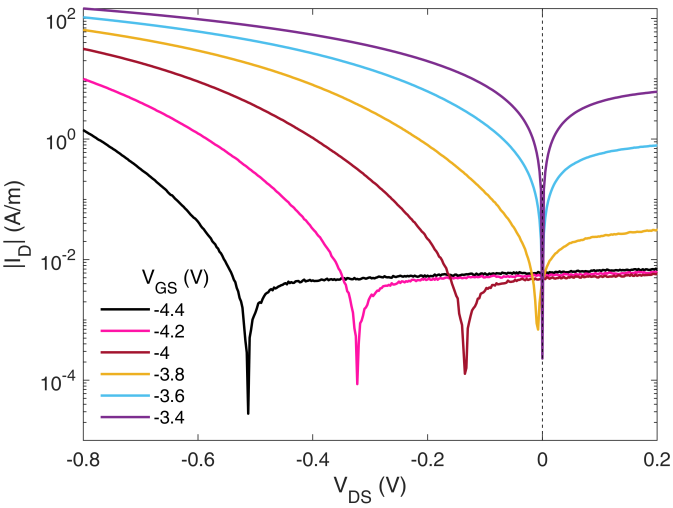

Fig. 9. Selected $|I_D| - V_{DS}$ characteristics curves of the device for over threshold (V_{GS}=-3.4 and -3.6 V) and subthreshold conditions ($V_{GS} = -3.8, -4, -4.2$ and -4.4 V). The data corresponds to a GaN-HEMT with L_G=250 nm and W=2×25 μm at 300 K.

Since such low-frequency response cannot be originated by the gate-drain-coupling, the explanation for this result must be elsewhere.

In the Fig. 5(b) for DI and 6 (b) for GI, the noise equivalent power (NEP) corresponding to each responsivity curve is presented for both schemes (assuming equilibrium thermal noise, NEP$_j$=$\sqrt{4k_BTR_D}/\beta_{vj}$, with j=d,g and R_D the resistance of the transistor). The lowest value of the NEP is found above threshold as a consequence of the smaller resistance, 5 pW/Hz$^{1/2}$ in DI (f=1 GHz) and 33.9 pW/Hz$^{1/2}$ (f=43 GHz) in GI. This latter value would be even better at higher frequencies, above the frequency limit of our equipment, since the responsivity is still increasing and the NEP decreasing. For subthreshold conditions, this figure of merit takes similar values for both configurations of RF injection, with its best value around 90 pW/Hz$^{1/2}$ obtained at low frequency and then increasing with the frequency roll-off of the responsivity.

The values of f_{3dB} for DI as a function of temperature are presented in Fig. 7 for three lengths of the gate, L_G. Note that f_{3dB} takes nearly constant values with V_{GS} both in the above threshold and in the subthreshold bias regions, with a distinct increase when entering the latter. However, this is only observed for T >200 K since for lower T the responsivity is null in the subthreshold region. In this temperature range f_{3dB} in both bias ranges increases when lowering T, saturating above threshold at about 45 GHz for ∼100 K. We attribute such increase of f_{3dB} to the enhancement of the mobility, which decreases the channel resistance.

In [18], we reported a generic high-frequency model of two-port RF detectors, based on static coefficients g_{ij} (defined as $g_{ij} = \partial^{(i+j)}I_D/\partial^i V_{GS}\partial^j V_{DS}$ and extracted from the measured I_D-V_{DS} curves) and measured S-parameters, able to replicate DI and GI responsivities by means of the following closed-form expressions:

$$\beta_{vd} = -\frac{R_0}{2g_{01}}\left(g_{20}\left|S_{12}\right|^2 + g_{02}\left|1+S_{22}\right|^2 + 2g_{11}\Re[S_{12}^*(1+S_{22})]\right), \quad (1)$$

$$\beta_{vg} = -\frac{R_0}{2g_{01}}\left(g_{20}\left|1+S_{11}\right|^2 + g_{02}\left|S_{21}\right|^2 + 2g_{11}\Re[S_{21}^*(1+S_{11})]\right), \quad (2)$$

where R_0 is the output impedance of the RF source.

Fig. 8 shows that for $V_{GS} > V_{th}$, g_{20} is null (due to the zero I_D bias conditions) and g_{02} and g_{11} have opposite signs and similar absolute values, with a maximum around V_{GS}=-3.23 V. Remarkably, due to the capacitive gate-drain coupling, at low frequency $S_{12} = S_{21} = 0$, so that g_{02} is the only significant parameter for β_{vd} and g_{20} for β_{vg}. The fact that g_{20}

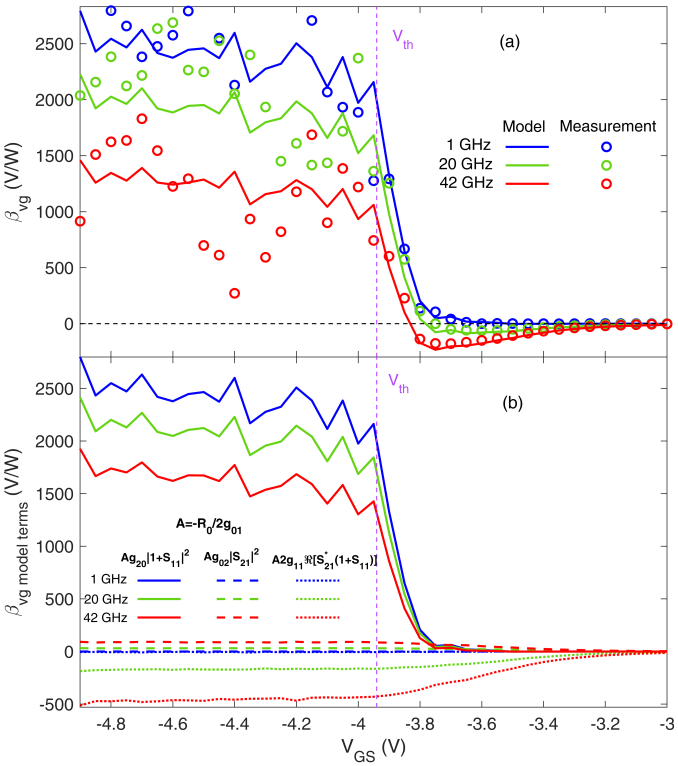

Fig. 10. (a) Comparison of the values of the ZC responsivity β_{vg} *vs.* V_{GS} obtained in the experiments (symbols) with those calculated with 2 (solid line) at 300 K for 1, 20 and 42 GHz. The dashed vertical line indicates the value of V_{th}. (b) Representation of the three terms of 2 for 1, 20 and 42 GHz.

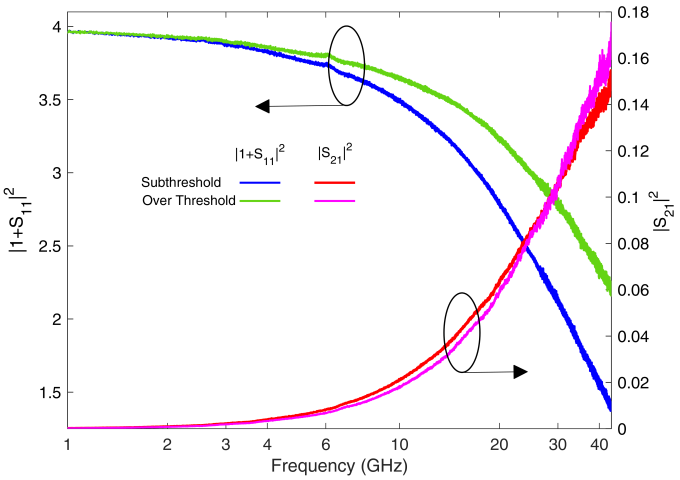

Fig. 11. $|1+S_{11}|^2$ (left y-axis) and S_{21} (right y-axis) as a function of frequency for bias points in subthreshold (V_{GS}=-4.28 V) and over threshold (V_{GS}=-3.61 V).

is null allows the model to clearly explain the low-frequency behavior of both responsivities above threshold, as well as the positive values obtained for β_{vd} and the negative ones for β_{vg}. At high frequency, S_{12}=S_{21} (the transistor acts as a passive network since V_{DS}=0) increase, and consequently the (negative) contribution of the g_{11} terms, so that the roll-off of β_{vd} and the increase of β_{vg} (over threshold) observed in Fig. 5(a) and Fig. 6(a), respectively, are also well captured by the model.

However, below threshold one would expect to find that $\beta_{vg} = 0$ at low frequency [14], contrary to what it is obtained in the experiments, Fig. 4(a). The explanation is that g_{20} is not zero in those conditions (see the zoom in the inset of Fig. 8). In fact, it reaches a value close to that of g_{02} and with the same sign, so that β_{vd} and β_{vg} exhibit a similar low-frequency behavior in the subthreshold region. The unexpected non-zero value of g_{20} occurs because for $V_{GS} < V_{th}$ the zero I_D point is shifted to negative values of V_{DS} (see the Fig. 9, with the $|I_D|$-V_{DS} curves of the transistor in log scale). This behavior is related to the gate-leakage current and ionization of deep donor-like traps. This ionization starts around T=200 K in C doped GaN [5], the technology of the device under test. As a consequence, since the $I_D = 0$ point depends on V_{GS}, the value of $g_{20} = \partial^2 I_D/\partial^2 V_{GS}$ is not null anymore for $V_{GS} < V_{th}$. The very good agreement found in the comparison of the experimental values of β_{vg} with those predicted using 2 for the whole V_{GS} range is shown in Fig. 10(a) at different frequencies. The corresponding terms of 2 are shown in Fig. 10(b). As expected, at 1 GHz (blue curves) only the term proportional to g_{20} contributes to the responsivity, since the second and third terms of 2 are null due to $S_{21} = 0$, as shown in Fig. 11, and therefore it is only significant in subthreshold conditions. When the frequency increases, S_{21} also increases and the second and third terms are no longer null, explaining the frequency roll off observed in Fig. 6(a) (blue curve) but the first term is still the dominant one in subthreshold. With the increase of frequency the first and the second terms add and counteract the effect of the third one. Finally, at f=42 GHz (red curves), even though $|1+S_{11}|^2$ is decreasing and the second and third terms increase, again the first term prevails. Therefore, below threshold the first term is always the dominant.

The roll-off of β_{vd} mentioned before, and observed in Fig. 4(a), is principally due to the fact that the coefficients g_{02} and g_{11} in 1 have opposite sign (see inset of Fig. 8). At high frequencies, the positive value of the third term increases and, when added to the negative value of the second term, it leads to a reduction of the (negative) responsivity. In subthreshold, the first term reinforces the second one, so that f_{3dB} increases.

IV. Conclusion

We have presented experimental results of zero-bias microwave power detection up to 43 GHz with GaN HEMTs both within the DI and GI configurations in a wide temperature range. While the dependencies of the detection on T, V_{GS} and frequency are well understood for $V_{GS} > V_{th}$, it is not the case in subthreshold conditions, where the drain self-bias plays a key role (mainly for T >200 K). In fact, it allowed us to explain the subthreshold behaviour of the responsivity β_{vg}. We remark that this mechanism also breaks the usual assumption that g_{20} is null in subthreshold, thus allowing to explain several initially puzzling results, mainly the non-zero values of the responsivity β_{vg} at low frequency (where the gate-drain coupling is null). With all the terms of equation 2 correctly taken into account, the dependence of the GI voltage responsivity on V_{GS} and frequency can be well reproduced by

the model. From a practical point of view, our zero-current results evidence that GI detection in the subthreshold region, in spite of increasing the responsivity at room temperature (and also increasing the f_{3dB} within DI conditions), leads to NEP values much higher than over threshold, thus degrading the detector sensibility.

REFERENCES

[1] J. Moon, D. Wong, M. Hu, P. Hashimoto, M. Antcliffe, C. McGuire, M. Micovic, and P. Willadson, "55% PAE and high power Ka-Band GaN HEMTs with linearized transconductance via n+ GaN source contact ledge," *IEEE Electron Device Lett.*, vol. 29, no. 8, pp. 834–837, Aug. 2008.

[2] K. Kikuchi, M. Nishihara, H. Yamamoto, T. Yamamoto, S. Mizuno, F. Yamaki, and S. Sano, "An 8.5–10.0 GHz 310 W GaN HEMT for radar applications," in *2014 IEEE MTT-S International Microwave Symposium (IMS2014)*, June 2014, pp. 1–4.

[3] P. Waltereit, W. Bronner, R. Quay, M. Dammann, M. Cäsar, S. Müller, R. Reiner, P. Brückner, R. Kiefer, F. Van Raay *et al.*, "GaN HEMTs and MMICs for space applications," *Semiconductor Sci. Technol.*, vol. 28, no. 7, p. 074010, June 2013.

[4] H. Hou, Z. Liu, J. Teng, T. Palacios, and S. Chua, "High temperature terahertz detectors realized by a GaN high electron mobility transistor," *Sci. Rep.*, vol. 7, no. 1, pp. 1–6, Apr. 2017.

[5] G. Paz-Martínez, I. Íñiguez-de-la Torre, H. Sánchez-Martín, J. A. Novoa-López, V. Hoel, Y. Cordier, J. Mateos, and T. González, "Temperature and gate-length dependence of subthreshold RF detection in GaN HEMTs," *Sensors*, vol. 22, no. 4, p. 1515, Feb. 2022.

[6] F. Aniel, G. Auton, D. Cumming, M. Feiginov, S. Gebert, T. González, C. Li, A. Lisauskas, H. Marinchio, J. Mateos *et al.*, "Terahertz electronic devices," in *Springer Handbook of Semiconductor Devices*. Springer, 2022, pp. 807–849.

[7] E. Javadi, D. B. But, K. Ikamas, J. Zdanevičius, W. Knap, and A. Lisauskas, "Sensitivity of field-effect transistor-based terahertz detectors," *Sensors*, vol. 21, no. 9, p. 2909, 2021.

[8] M. S. Nazir, P. Kushwaha, A. Pampori, S. A. Ahsan, and Y. S. Chauhan, "Electrical characterization and modeling of GaN HEMTs at cryogenic temperatures," *IEEE Trans. Electron Devices*, vol. 69, no. 11, pp. 6016–6022, 2022.

[9] Y. Liang, H. Chen, H. Xing, T. Cai, Y. Ye, H. Liang, X. Xia, W. Guo, and N. Xu, "The interface trap analysis of AlGaN/GaN high electron mobility transistors with temperature based on conductance method," vol. 2248, no. 1, p. 012016, 2022.

[10] G. Paz-Martínez, I. Íñiguez-de-la Torre, H. Sánchez-Martín, T. González, and J. Mateos, "Analysis of GaN-based HEMTs operating as RF detectors over a wide temperature range," *IEEE Trans. Microw. Theory Techn.*, vol. 71, no. 7, pp. 3126–3135, 2023.

[11] W. Knap, V. Kachorovskii, Y. Deng, S. Rumyantsev, J.-Q. Lü, R. Gaska, M. Shur, G. Simin, X. Hu, M. A. Khan *et al.*, "Nonresonant detection of terahertz radiation in field effect transistors," *J. Appl. Phys.*, vol. 91, no. 11, pp. 9346–9353, Jun. 2002.

[12] H. Kojima and T. Asano, "Impact of subthreshold slope on sensitivity of square law detector for high frequency radio wave detection," *Jpn. J. Appl. Phys.*, vol. 58, no. SB, p. SBBL05, Mar. 2019.

[13] M. Sakowicz, M. Lifshits, O. Klimenko, F. Schuster, D. Coquillat, F. Teppe, and W. Knap, "Terahertz responsivity of field effect transistors versus their static channel conductivity and loading effects," *J. Appl. Phys.*, vol. 110, no. 5, p. 054512, Sept. 2011.

[14] M. A. Andersson and J. Stake, "An accurate empirical model based on volterra series for FET power detectors," *IEEE Trans. Microw. Theory Techn.*, vol. 64, no. 5, pp. 1431–1441, May 2016.

[15] M. I. W. Khan, S. Kim, D.-W. Park, H.-J. Kim, S.-K. Han, and S.-G. Lee, "Nonlinear analysis of nonresonant thz response of MOSFET and implementation of a high-responsivity cross-coupled thz detector," *IEEE Trans. Terahertz Sci. Technol.*, vol. 8, no. 1, pp. 108–120, Jan. 2017.

[16] S. M. Homayouni, D. M.-P. Schreurs, G. Crupi, and B. K. Nauwelaers, "Technology-independent non-quasi-static table-based nonlinear model generation," *IEEE Trans. Microw. Theory Techn.*, vol. 57, no. 12, pp. 2845–2852, 2009.

[17] G. Paz-Martínez, I. Íñiguez-de-la Torre, H. Sánchez-Martín, B. García-Vasallo, N. Wichmann, T. González, and J. Mateos, "Comparison of GaN and InGaAs high electron mobility transistors as zero-bias microwave detectors," *J. Appl. Phys.*, vol. 132, no. 13, p. 134501, Sept. 2022.

[18] G. Paz-Martínez, P. Artillan, J. Mateos, E. Rochefeuille, T. González, and I. Íñiguez-de-la Torre, "A closed-form expression for the frequency dependent microwave responsivity of transistors based on the I-V curve and S-Parameters," *IEEE Trans. Microw. Theory Techn.* [Online]. Available: https://doi.org/10.1109/TMTT.2023.3291391